Microchemical Journal 216 (2025) 114645

Contents lists available at ScienceDirect

Microchemical Journal

journal homepage: www.elsevier.com/locate/microc

Nanoengineered electrochemical sensor for trace-level monitoring of perfluorooctanoic acid in aqueous environments using electroactive molecularly imprinted nanoparticles

Marco Costa [a,*], Sabrina Di Masi [a,*], Christopher Zaleski [b], Alvaro Garcia Cruz [b], Erik Beij [c], Jeroen Peters [c], Sergey A. Piletsky [b], Cosimino Malitesta [a], Giuseppe Egidio De Benedetto [d]

[a] Laboratory of Analytical Chemistry, Department of Biological and Environmental Sciences and Technologies, University of Salento, 73100 Lecce, Italy
[b] Department of Chemistry, University of Leicester, University Rd, LE1 7RH Leicester, UK
[c] Wageningen Food Safety Research, Akkermaalsbos 2, 6708, WB, Wageningen, the Netherlands
[d] Laboratory of Analytical and Isotopic Mass Spectrometry, Department of Cultural Heritage, University of Salento, 73100 Lecce, Italy

ARTICLE INFO

Keywords:
Electrochemical sensor
MIP
Solid-phase polymerization
Experimental design
Perfluoroalkyl compounds
Chemometric optimization

ABSTRACT

A new voltammetric sensor was developed for the sensitive and selective detection of perfluorooctanoic acid (PFOA) in water. The sensor is based on molecularly imprinted polymer nanoparticles (nanoMIPs) labelled with a redox-active moiety, which imparts electrochemical properties to the polymer. These nanoMIPs were synthesized using solid-phase polymerization, with their size optimized through chemometric modelling, including functional monomer screening and recognition cavity design. The optimization aimed to minimize the nanoMIP size, which is directly influenced by the amount of polymerization initiator, and to enhance sensor response. A commercially available screen-printed platinum electrode (SPPtE) served as the transducer element, functionalized with APTES to enable covalent attachment of nanoMIPs. The sensor demonstrated a detection capability for PFOA concentrations as low as 0.40 ± 0.03 pg mL^{-1}, and a linear response up to 7.5 pg mL^{-1}. Furthermore, the calibration curve was fitted to the Michaelis-Menten model, thanks to the allosteric behavior of the nanoparticles mimicking enzyme-substrate interactions. A Km of 4.34 pg mL^{-1} for MIP and 17.73 pg mL^{-1} for the control were obtained. Its selectivity was evaluated in samples containing structurally similar PFAS compounds, showing high effectiveness also in contaminated water. Additionally, a successful regeneration strategy was developed, enabling the sensor to be used across at least 3 work cycles. The successful adaptation of the developed method to a handheld miniaturized potentiostat connected to an Android phone enables on-site inspections of surface waters at the point of need.

1. Introduction

Perfluorooctanoic acid (PFOA), a member of the perfluorinated chemicals (PFCs) class, is a persistent organic pollutant that has garnered significant attention due to its extensive environmental presence and associated health risks. PFOA is known for its resistance to degradation, leading to its accumulation in the environment and living organisms. This persistence raises concerns about its potential to cause adverse health effects, including developmental toxicity, and an increased risk of certain cancers [1]. Perfluoroalkyl substances (PFAS) contamination mainly originates from industrial activities and sources such as sewage, landfills, air emissions, airports, and fire training sites [2] and it is a global issue [3]. Due to their strong C—F bonds, PFAS are highly persistent in the environment, resisting biodegradation [4] and photodegradation [5]. The "Forever Pollution Project" identified over 22,000 contaminated sites across Europe. PFOA, typically present as the perfluorooctanoate ion (pKa ≈ 0), has high water solubility (9500 mg/L) and a CMC of 3460 mg/L, and is considered a marker of general PFAS pollution. The presence of PFOA can be indicative of general PFAS contamination, including PFOS, see Table **S1** about surface water/groundwater, drinking water, and bottled water [6,7].

Liquid chromatography-mass spectrometry (LC-MS), using various mass analyzers (single/triple quadrupole mass spectrometry and ion-trap detectors) or gas chromatography–mass spectrometry (GC–MS)

* Corresponding authors.
E-mail addresses: marco.costa@unisalento.it (M. Costa), sabrina.dimasi@unisalento.it (S. Di Masi).

https://doi.org/10.1016/j.microc.2025.114645
Received 23 May 2025; Received in revised form 17 July 2025; Accepted 21 July 2025
Available online 22 July 2025

are commonly employed to identify PFAS [8]. Although these methods offer high performance for the detection of PFAS, these techniques have some practical disadvantages, such as high costs and the need for trained personnel to generate and interpret the data. In contrast, chemical sensors, characterized by fast response times and high sensitivities, represent a more practical alternative for on-site application [9,10]. They can be designed as portable devices and fabricated using low-cost manufacturing processes [11,12], allowing for a green approach [13–15] are also easy-to-use, making them more suitable for non-expert operators.

In this study, we report the development of a novel electroactive nanoMIPs-based chemosensor for the monitoring of PFOA in water matrices. Their synthesis has been optimized to produce particles about 100 nm in size to take advantage of the high surface area-to-volume ratio, which significantly enhances reactivity and interaction with target molecules.

The resulting PFOA nanoMIPs were immobilized onto functionalized screen-printed electrodes permitting fast and accurate detection of PFOA, at low ng mL^{-1} (ppb) concentrations. The sensing mechanism is based on is similar to the principle of allosteric regulation in enzymes. Upon binding to the analyte, the polymer undergoes conformational changes that expose additional ferrocene monomer groups. This process increases the electron transport rate and activates the electroactive regions of the redox label. As a result, the sensor current varies with the analyte concentration, enabling detection directly via buffer [16]. In addition, a regeneration strategy has been developed for the re-use of the SPE sensors with a consistent level of performance. The performance of the nanoMIPs based-sensor has been assessed and the accurate detection of PFOA in a real sample has been demonstrated. The implementation of the sensor on a handheld miniaturized potentiostat connected to an Android phone demonstrated the feasibility of monitoring at the point of need. As a result, the developed sensor has the potential to make a significant contribution to environmental protection and public health safeguard.

2. Material and methods

2.1. Chemicals

Glass beads (150 μm) were purchased from Microbeads AG (Gebenstorf, Switzerland). PFOA (95 %) and related PFAS compounds PFOS (≥98.0 %), perfluoropentanoic acid (PFPeA) (97 %), perfluorononanoic acid (PFNA) (≥97 %), perfluorobutanesulfonic acid (PFBS) (98 %) and calcium carbonate were purchased from Sigma Aldrich (Milano, Italy). Itaconic acid (ITA), ethylene glycol dimethacrylate (EGDMA), pentaerythritol tetrakis (3-mercaptopropionate) (PETMP), ferrocenylmethyl methacrylate (FcMMA), trimethylolpropane trimethacrylate (TRIM), 2-hydroxyethyl methacrylate (HEMA), 1-ethyl-3-(3-dimethylaminopropyl)carbodiimide (EDC), N-hydroxysuccinimide (NHS), 3-aminopropyltriethoxysilane (APTES), glutaric dialdehyde (50 % solution), trifluoroacetic acid (TFA), acetic anhydride, 1,2-bis(triethoxysilyl)ethane, benzyl diethyldithiocarbamate (iniferter) were obtained from Sigma-Aldrich (UK). PBS tablets (phosphate buffered saline pH 7.4) (dimethylformamide (DMF), acetonitrile, ethanol, toluene and acetone were from Fisher Scientific, UK. Acetate buffer solutions (5 mM, pH = 3.6 and 4.5) were prepared from glacial acetic acid and NaOH (both from Honeywell, Italy), phosphate buffer (5 mM, pH 6.0) from sodium phosphate monobasic monohydrate and sodium phosphate dibasic heptahydrate (Fisher Bioreagent, Italy). Cadmium nitrate tetrahydrate (98 %) and magnesium nitrate were purchased from Merck (Milano, Italy). Uric acid (UA) was purchased from Carlo Erba, Italy.

2.2. Preparation of MIPs nanoparticles

2.2.1. Molecular modelling

Molecular modelling was conducted using an HP Elite-Desk equipped with two Intel Core™ Duo CPU E8400 processors, each running at 3GHz, and operated on the CentOS Linux 7 operating system. Sybil™ version 7.3 (Tripos Inc.) software within a Gnome 2.28.2 (Linux) environment was used for to study the approach of molecular modelling, before starting the synthetic procedure to screen for complexation between the functional monomers and the target. Furthermore, AutoDock Vina, an open-source docking application, was used to verify the results. Sybyl-X 2.0 was used for energy minimisation and to create 3D models of the molecules. Each molecule energy was first minimized to provide a gradient of 0.01 kcal/mol $Å^{-2}$ using the default Tripos force field and a dielectric constant of 78.4 (water, pH 7). Additionally, the geometry of each monomer had been previously minimized and refined using the Powell method, Force Fields (Tripos), and Charges (Gasteiger-Huckel) to reach a minimum energy of 0.001 kcal/mol. Afterwards, 50 ns of molecular dynamics (MD) simulations were run with a 10,000 iteration limit.

2.2.2. Glass beads functionalization

The solid support functionalization procedure was adapted from an earlier study [17]. At first, 200 g glass beads (GB) were activated with NaOH (4 M, 1 L) for 15 min, then rinsed thoroughly through a sintered disc filter funnel with deionized water, PBS (pH 7.4) and anhydrous acetone. GB were then dried in oven (150 °C) for 50 min. Silanization was performed by incubating GB for 6 h in a solution of dry toluene (182 mL), 1,2-bis(triethoxysilyl)ethane (6 mL), and APTES (12 mL) dissolved in ethanol (5 % *v*/v), respectively. Finally, they were rinsed with warm (70 °C) toluene (200 mL) and anhydrous acetone. Anchoring PFOA target molecule to silanized GB was performed as described earlier [18]. Briefly, PFOA (10 mM) was immobilized on 30 g silanized-GB via carbodiimide using EDC/NHS (1:1.5 M ratio) in PBS (5 mM, pH 7.4) for 1 h under stirring. Next, the unreacted primary amine groups were deactivated using 1.5 mL acetic anhydride and 58 mL acetonitrile, for 30 min while stirring. Dry acetone was used to wash the GB, followed by vacuum drying. The resulting PFOA-GBs were used for the nanoMIPs synthesis.

2.2.3. Synthesis by solid phase polymerization (PFOA-nanoMIPs)

Photo-polymerization was used for the synthesis of perfluorooctanoic acid-imprinted polymer nanoparticles (PFOA-nanoMIPs), in the presence of PFOA-GB. The nanoMIPs polymerization mixture comprised: ITA (0.325 g, 50 mM) and HEMA (0.325 g, 50 mM) as functional monomers, FcMMA (0.04 g, 3 mM) as redox marker, benzyl diethyldithiocarbamate as initiator (0.147 g, 12.3 mM), PETMP (0.04 g, 2.0 mM) as chain-transfer agent, and EGDMA (0.502 g, 50.6 mM) and TRIM (0.846 g, 50.0 mM) as cross-linkers. Acetonitrile (50 mL) was used for dissolving all polymerization reagents. The mixture was sonicated and degassed for fifteen minutes, then added into a flat-bottom crystallising dish, which contained the dried beads. The polymerization was started by exposing the mixture to UV light (UV-lamp, 0.5 W cm − 1, 4 × 15 W, Philips HB171/A, Hamburg, Germany) for three minutes. The high-affinity nanoMIPs were eluted using 50 mL of ethanol at 70 °C. The nanoMIPs suspension was collected in a round bottom flask, concentrated by evaporation using a rotary evaporator (pressure fixed at 175 mbar at 60 °C) until reaching a volume of approximately 5 mL. This suspension can be freeze-dried and recovered before use to ensure a better preservation and stability over time. The nanoparticles used as a negative control were prepared with the same protocol using trifluoroacetic acid as a template (TFA or control nanoMIPS). For characterizations and subsequent studies, a concentration of 0.2 mg/mL nanoMIPs in ethanol was used.

2.3. Optimisation of nanoMIPs synthesis

Experimental design was used to study the influence of the polymerization mixture on the size of the nanoparticles and to minimize their dimensions. First, a definitive screening design was selected to find

significant factors and interactions that affect nanoMIP preparation. ITA, HEMA, ferrocene methylmethacrylate, TRIM, PETMP, iniferter concentrations (mM) were considered in this design (17 runs) and the resulting experimental matrix is in **Table S2**, respectively. The response was the dimensional distribution of prepared nanoMIPs measured by dynamic light scattering (DLS). Afterwards, a response surface methodology (RSM) based on central composite design (CCD) was built for significant variables ($p < 0.05$) (see **Table S3** and **S4**). The goal was to minimize particle size, with a target of 100 nm. Mathematical models and experimental fitting were built and performed by using MODDE® software.

2.4. Characterisation of PFOA-nanoMIPs and control

PFOA-nanoMIPs were characterized by means of various analytical tools. DLS equipped with Zetasizer Nano (Malvern Instruments Ltd., UK) was used for the determination of the size of the nanoparticles. For these measurements, 100 μL of nanoparticles (0.2 mg/mL) were diluted in 900 μL of water and sonicated for 1 min. Fourier-transform infrared (FTIR) spectra were recorded using an ALPHA II (Bruker Optics) instrument to characterise nanoMIPs, silanized GBs before and after polymerization, and after elution of nanoparticles. A JEOL JEM-1400 Transmission electron microscope with an accelerating voltage of 120 kV was used to analyse morphology of the nanoparticles whereas images were taken with an EMSIS Xarosa 20MP digital camera employing Radius software. A hydrophilic surface carbon film copper grids was produced by a 30-s plasma discharge. After a minute a 2 μL solution of nanoparticles was added on the surface-treated grid and the dispersion in excess was wiped off with filter paper. Next, the grid was filled with 2 μL of a uranyl formate (0.1 % *w/v*) aqueous solution (negative stain) before measurements.

2.5. Preparation of sensor

2.5.1. Electrode functionalisation

The screen-printed platinum electrodes (SPPtE, Dropsens DRP-550, Metrohm, Runcorn, UK) with a platinum working electrode (4 mm diameter), a platinum counter electrode, and silver-silver chloride as a pseudo-reference electrode on a planar ceramic support (3.3 × 1 cm) served as the surface for the preparation of the electrochemical sensors. A PalmSens potentiostat (PalmSens4, Dordrecht, The Netherlands) equipped with PSTrace for data collection and analysis was used to carry out the electrochemical experiments. A total of 5 μL of 3-aminopropyltriethoxysilane (APTES, 5 % in ethanol) was drop-cast onto the SPPtE surface in three successive applications. The surface was then dried in an oven at 150 °C for one hour to facilitate covalent functionalization of the surface. The modified sensor was then left to air dry for 8 h. After that, PBS (5 mM, pH 7.4) was used to gently rinse APTES/SPPtE.

2.5.2. NanoMIPs immobilization

The nanoMIPs solution was sonicated for 2 min to prevent nanoparticle aggregation [19]. The immobilization of the nanoMIPs on the modified electrode surface was performed using EDC/NHS coupling. A solution of PBS (5 mM, pH 7.4) comprising 80 μL of nanoMIPs (0.2 mg/mL), 10 μL of EDC (30 mM) and 10 μL of NHS (60 mM) was dropped onto APTES/SPPtE for 40 min. Then, the PFOA-nanoMIP sensor was gently rinsed with PBS to remove non-immobilized nanoMIPs.

2.5.3. Electrochemical characterisation of sensors

Cyclic voltammetry (CV) and differential pulse voltammetry (DPV) measurements were used to electrochemically characterise the developed sensors at each stage of electrode modification: bare SPPtE, APTES/SPPtE, and PFOA-nanoMIPs sensors in 5 mM PBS pH 7.4 with 10 mM $Fe(CN)_6^{3-}$ as the electrochemical redox probe. Similar measurements were also performed without the ferrocyanide. CV was performed at a scan rate of 50 mV/s in the potential range − 0.1 V - +0.8 V vs. pseudo Ag reference electrode. DP voltammograms were recorded in the potential range of −0.15 V to +0.4 V vs. pseudo Ag reference electrode with potential step, 4.95 mV; modulation amplitude, 0.2 V; pulse duration, 20 ms; scan rate, 50 mV/s.

2.6. PFOA sensing and sensor validation

The electrochemical responses of PFOA-nanoMIP and control sensors were measured by differential pulse voltammetry (DPV) ($n = 3$) in the potential range between −0.15 V and + 0.4 V (vs. pseudo Ag reference), with a modulation amplitude of 0.2 V, step potential of 4.95 mV, pulse duration of 20 ms, and scan rate of 50 mV/s. First, the baseline current in PBS (5 mM, pH = 7.4) was measured, followed by different concentrations (1.0–100 pg mL^{-1}) of PFOA dissolved in PBS. Voltammograms were recorded after an incubation time of 10 min. The measured currents were subtracted from the baseline current to obtain the analytical signal. The electrode surface was carefully cleaned with MilliQ water following each measurement. pH effect was studied in the range 3.6–7.4 as follows: the baseline current was recorded in a selected pH buffer by differential pulse voltammetry (DPV) of the sensor after the immobilization of nanoparticles. Subsequently, a 100 μL droplet of the PFOA solution was applied onto the sensor and incubated for 10 min. Next, the droplet containing the PFOA was removed, and the sensor surface was washed thoroughly with deionized water. DPV responses were then recorded using a buffer solution at the same pH as previously selected and the measured current was subtracted from the baseline current to get the sensor's response. The obtained calibration curve was then adapted to the Michaelis–Menten fitting given the similar behavior of MIP with enzymatic bonds [10,20–22]. To investigate the selectivity of the sensor, mixtures of 4 pg mL^{-1} PFOA containing 40 pg mL^{-1} of some PFAS (PFOS, PFPeA, PFNA, PFBS) were tested for their cross-reactivity. The recovery of the sensor at different PFOA levels was determined in tap water diluted 1:10 with PBS: the solutions were stirred and, after the baseline measurement, spiked with PFOA. The responses were recorded after 10 min incubation as described previously. A contaminated surface water sample collected near a Dutch industrial site was also analyzed. Before measurement, the sample was diluted 10 times with PBS to bring its concentration in the linear range of the sensor.

3. Results and discussion

3.1. Molecular modelling

A molecular modelling was explored to identify the most favourable complex formation between selected monomers and the PFOA target [23]. The Sybyl method was employed to predict electronegativity sites through energy surface mapping, enabling the identification of high-probability interaction sites. This approach guided the design of the nanoMIP recognition site. A stochastic loop evaluated monomer-target interactions, with successful interactions recorded in 3D for subsequent docking cycles and optimized geometry. Sybyl employs molecular mechanics to calculate molecular properties, utilizing atom-like particles, charge distributions, and classical potentials. Due to methodological constraints and computational limitations, the analysis was limited to one-to-one molecule interactions at a time. The Leapfrog algorithm within Sybyl enables virtual screening of a monomer library by positioning functional monomers around the target molecule. It calculates potential energy, electronegativity, and interactions, and evaluates binding scores to identify optimal candidates. Favourable interactions are indicated by negative energy values. The monomer library consists of 20 functional monomers with vinyl polymerizable units and interactive functional groups. These monomers, which are commercially available and highly polymerizable, are widely used in molecular imprinting applications.

The optimized structures are shown in **Fig. S1**, indicating that both ITA and HEM monomers can form a robust complex with PFOA. An

acidic monomer is typically not the ideal choice for binding an acidic analyte due to the potential for charge repulsion between similarly charged acidic groups. Instead, complementary monomers with basic (e.g., amine) or neutral functional groups are generally more suitable for binding acidic analytes. Nevertheless, monomers such as ITA and HEM can form stronger interactions with PFOA through mechanisms like hydrogen bonding, electrostatic interactions, or van der Waals forces. The interaction between PFOA and ITA arises from the interaction of their carboxylic groups. In the complex, which has a binding energy of −11.96 kcal/mol, a hydrogen bond forms between the carboxyl group of PFOA and the hydroxyl group of ITA. Additionally, another complex can be formed between the carboxyl groups, with a binding energy of −6.41 kcal/mol, as illustrated in **Fig. S2**. On the other hand, PFOA exhibits hydrophobic interactions with the hydroxyl groups of HEM, resulting in an interaction of −7.43 kcal/mol. To confirm the results, AutoDock Vina, an open-source docking tool, was utilized. This tool randomly placed monomer copies to ensure accurate outcomes. Despite the practicality of Sybyl, AutoDock lacks a rational basis for initial placement. However, replicating AutoDock with the MMFF94 force field consistently yielded results, with MMFF94 being suitable for molecular dynamics and geometry optimization in condensed-phase processes. Based on these results, the monomers were chosen for the nanoparticles synthesis.

3.2. Optimisation of nanoMIPs preparation

To develop sensors based on MIPs as recognition molecules, optimisation is crucial to obtain expected performances [24]. Our focus relied on optimisation of size distribution to better accommodate nanoMIPs onto electrode surfaces. Achieving smaller nanoparticle sizes is particularly advantageous as it addresses challenges related to sensitivity and selectivity toward specific targets. This size reduction not only increases the surface area but also indirectly minimizes non-specific binding sites [25]. This is crucial in mitigating interactions with interfering molecules that share physico-chemical properties similar to the target. In fact, the dimensions and distribution of imprinted nanoparticles play a crucial role in determining their properties, with several factors affecting these characteristics, such as polymer molecular weight, surface tension, conductivity, polymer concentration, acid concentration, process parameters, and the distance between electrodes and the crosslinker [26–30]. A screening design was carried out to study the factors influencing the production of the nanoMIPs, which can be tuned through the polymerization process whereas a central composite design modelled the optimal conditions to obtain smaller and reproducible nanoparticles. At first, the influence of polymerization reagents to impart nanoscale-sized particles was studied (**Table S2**). Responses were collected by DLS measurement for each experimental trial of the mathematical model. As shown in the dataset (**Table S2**), responses exhibited a bell-shaped normal distribution. Coefficient plot (**Fig. S3**) shows ferrocene methyl methacrylate and benzyl diethyldithiocarbamate (initiator) as the main factors affecting nanoMIPs size. PEMPT and EGDMA were significant as well but to a minor extent. These results are not unexpected as PETMP is reported to favour plasmon coupling [31], whereas EGDMA affects size [32]. As to initiator, it plays a role in the solid phase synthesis of nanoparticles by enabling control of polymerization, making nanoparticles uniform, and ensuring compatibility with solid supports. These factors collectively contribute to the effectiveness of initiators in synthesizing nanoparticles in a solid-phase environment. Ferrocene methyl methacrylate and iniferter concentrations (see **Table S2**), which appeared the most significant variables on produced size nanoMIPs, were then subjected to RSM optimisation by a central composite design (CCD) Experimental matrix consisting of 10 plus 3 center points and relevant responses are collected in **Table S3** and **S4**. Reproducibility is very satisfactory, as shown by the small variation in response at the central point (**Fig. S6**). The model, whose results are shown in **Fig. S7**, fits well with the experimental data and has a great predictive capability, as confirmed by the high values of R2 and Q2, respectively (**Fig. S8**). Therefore, the optimized concentrations (3 mM FcMMA and 12.28 mM iniferter) were used for the synthesis of the nanoparticles. With these conditions, the solid-phase polymerization process yielded 290–300 mg of nanoMIP per 25 g of analyte-immobilized glass beads with. However, the yield decreased with repeated reuse of the solid phase, i.e. PFOA-GBs, and subsequent washing steps. Therefore, after the third reuse cycle, to avoid loss of chemicals, it is recommended to replace the solid phase with a freshly modified one.

3.3. Characterisation of imprinted nanoparticles

The hydrodynamic size of PFOA-nanoMIPs and TFA-nanoMIPs (control) were determined by DLS measurement ($n = 3$). Fig. 1A shows a spherical-shaped particle diameter of 106.2 ± 0.7 nm for PFOA-nanoMIPs and 78.34 ± 7.7 nm for control (Fig. 1B). The polydispersity index (PDI) was 0.196, which represents an acceptable value, considering that a PDI value around 0.2 for nanoMIPs indicates that the particles are homogeneously distributed [33]. The TEM images for the nanoMIPs showed spherical particles with a size of approximately 105 nm as shown in Fig. 1C, which agreed with that obtained by DLS measurements and predicted by RSM modelling. FT-IR measurements were carried out to characterise glass beads functionalized with the target template and to control the elution of nanoparticles. **Fig. S9A** shows that the spectra obtained between before polymerization and after the elution procedure overlap, indicating the total recovery of the nanoparticles from the template. The most significant peaks in the FT-IR spectrum of the nanoparticles (**Fig. S9B**) are due to the carboxylic groups around 1670 cm^{-1} and the aliphatic C—H and C—C stretching at about 3000 and 1500 cm^{-1}, respectively.

3.4. Electrode functionalisation

SPPtE electrodes were functionalized to allow anchoring of nanoMIPs to the sensing surface. The functionalisation was performed by drop casting 5 μL of a 5 % APTES in ethanol solution. The functionalized electrode exposes the -NH_2 groups, available for EDC/NHS coupling reaction with the carboxyl groups of the NPs, resulting in stable amide bonding [34,35]. Electrode modification was monitored by comparing CVs and EIS spectra recorded on the bare SPPtE and after APTES/SPPtE, respectively. CV in **Fig. S10C** shows the decrease in current on the electrode surface after the formation of a layer of APTES, indicating the successful functionalization of the SPE. At the same time, EIS (**Fig. S10B**) shows the measured increase in impedance. EIS spectrum was fitted with Randles circuit demonstrating that, before the APTES functionalization, the R_{et} value of bare SPPtE was 72 Ω. The modification of the electrodes is confirmed by the increase in resistance, up to about 2055 Ω, due to the APTES layer. Also, the electrochemical behavior changed after the functionalization of the sensor with APTES layer (**Fig. S10A**). After the immobilization of nanoparticles, anchored by EDC/NHS coupling mechanism the resistance was 2392 Ω. After the incubation with 100 pg mL^{-1} PFOA standard solution, the impendence measured by EIS was 5294 Ω, with an increase of 2902 Ω in comparison to the sensor with no analyte.

3.5. Analytical performances of optimized sensor

The analytical performance of the nanoMIPs sensor was evaluated by measuring the sensor response to PFOA by DPV (Fig. 2A). The peak current at +0.15 V is due to the presence of ferrocene redox label in the nanoMIPs. Basically, the response of the electroactive nanoparticles following binding of the target to the recognition sites involves conformational changes of the nanoMIPs which alters the electrochemical activity of the polymer [16]. This behavior is similar to the allosteric effect in proteins which are able to change their conformation

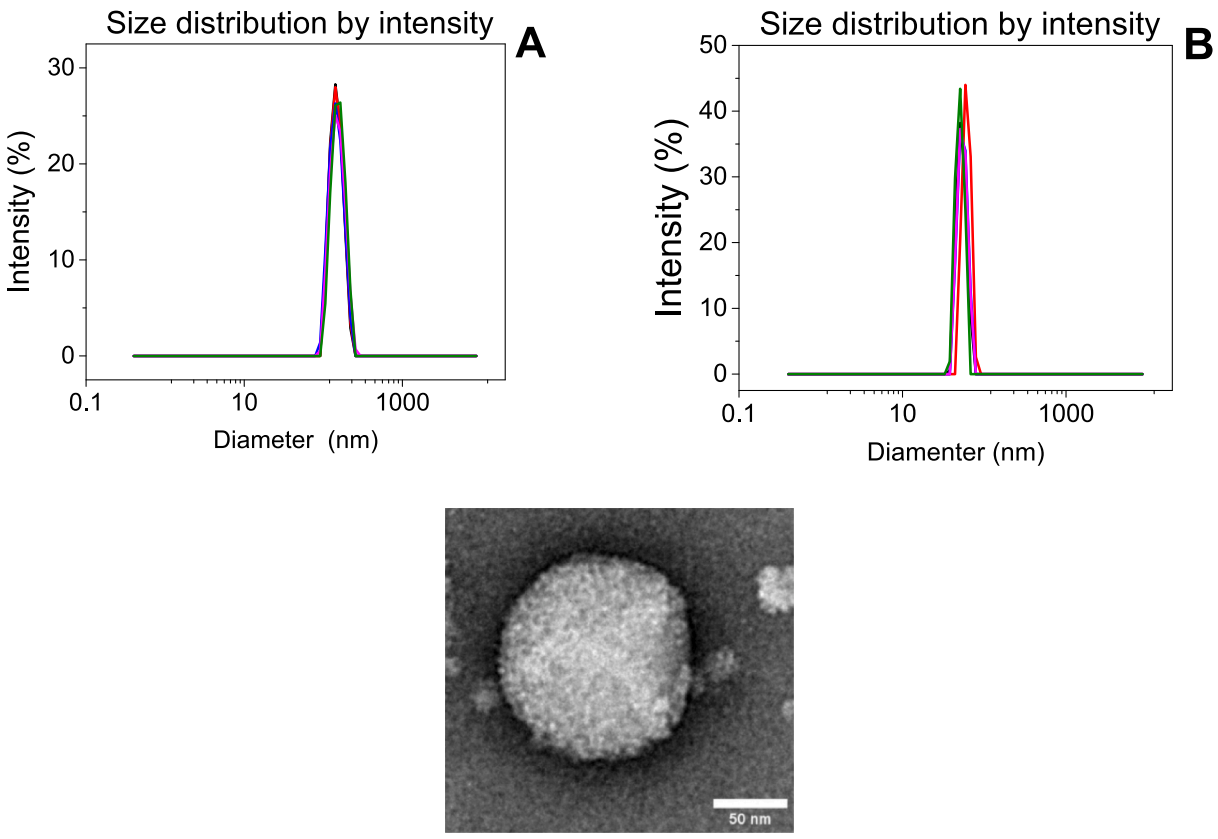

Fig. 1. (A) Size distribution by intensity of nanoMIPs vs PFOA obtained by DLS. (B) Size distribution by intensity of nanoparticles used as control (TFA nanoMIPs) obtained by DLS. (C) TEM images for nanoMIP specific for PFOA with a scale bar at 50 nm. (D) CV performed for bare SPPtE (black line) and after APTES functionalization (red line) in PBS (5 mM, pH 7.4) containing 10 mM $Fe(CN)_6^{3-}$, 0.1 M KCl. (E) Nyquist plots for bare SPPtE (black), after APTES functionalization (blue), after nanoMIPs immobilization (purple) and after sensor test at 100 pg mL^{-1} (red). (For interpretation of the references to colour in this figure legend, the reader is referred to the web version of this article.)

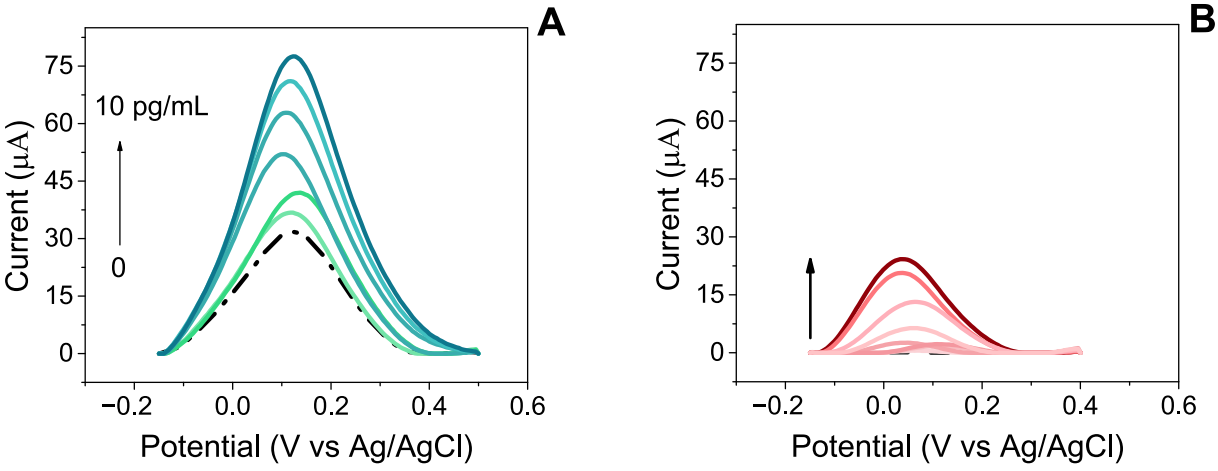

Fig. 2. DPV measurements, recorded in PBS (5 mM, pH 7.4), for (A) nanoMIPs-PFOA sensor and (B) negative control, after exposure to 1, 2, 3, 4, 5, 7.5, 10 pg mL^{-1} PFOA standard solutions in PBS (5 mM, pH 7.4).

following interaction with ligands [36]. Solid phase synthesis of nanoMIPs does not allow obtaining non-imprinted nanoparticles free of a target [37]. Therefore, the negative control sensor for this study was produced by immobilising nanoMIPs synthesized using trifluoroacetic acid as a template. The responses to PFOA of the control sensor (Fig. 2B) demonstrate the effectiveness of the solid phase polymerization to produce PFOA-nanoMIPs, demonstrated clearly by lower the peak currents.

As pH can influence the binding affinity and recognition ability [38], its effect in the range 3.6–7.4 was studied. The sensor response to 5 pg mL^{-1} of PFOA was measured at this pH interval with the optimal response obtained at pH 7.4 (**Fig. S11**). Therefore, all subsequent measurements were conducted at this specific pH value. The instrumental response to a set of PFOA standard solutions in PBS (5 mM, pH 7.4) with concentrations between 100 and 1 pg mL^{-1} was recorded for both sensor and control (Fig. 3A). The fitting with the Michaelis-Menten model described a calibration curve and, subsequently, both were

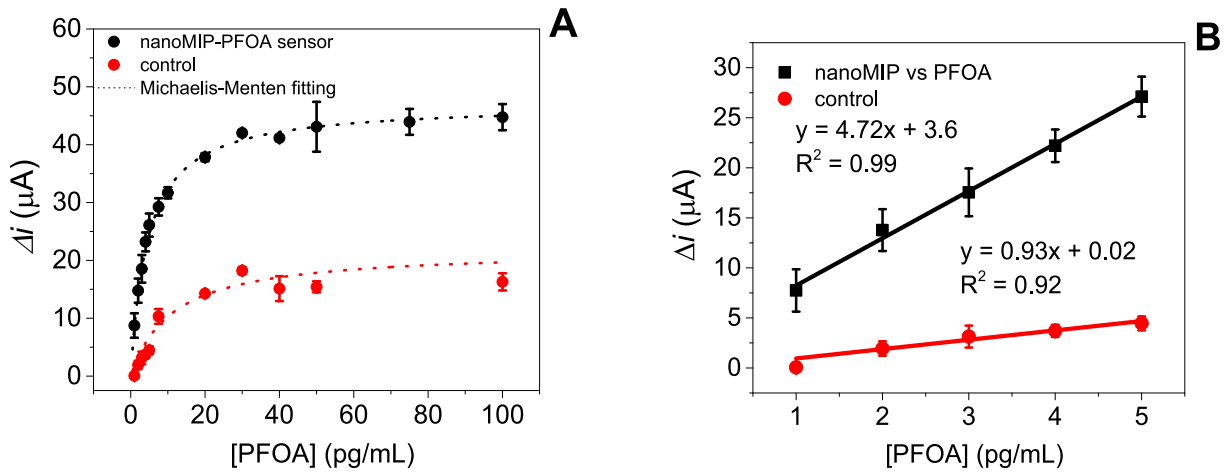

Fig. 3. (A) Response of both the nanoMIP-PFOA sensor (black) and the negative control (TFA) nano-MIP sensor (red) to PFOA at concentration range from 1 up to 100 pg mL^{-1}. (B) Calibration curve with least squares fitting of nanoMIP-PFOA sensor (black line) and negative control (red line) in the linear range of the analysis. Error bars represent the standard deviation of three replicates ($n = 3$). DPV measurements were carried out in PBS (5 mM, pH 7.4). (For interpretation of the references to colour in this figure legend, the reader is referred to the web version of this article.)

adapted with the Lineweaver-Burk (**Fig. S12**) plot from which the parameters Δi_{max} and Km were obtained. The fit with the Michaelis-Menten model results a Δi_{max} of 46.72 μA and Km of 4.34 pg mL^{-1}. Furthermore, R^2 of 0.998 confirms the suitability of the Michaelis-Menten model to describe the binding behavior of the MIP toward the target analyte. On the contrary, the control showed a higher Km of 31.01 pg mL^{-1}, hence a weaker affinity for the analyte compared to MIP, highlights its limited binding capacity. The sensor based on nanoMIPs had a linear response up to 7.5 pg mL^{-1} ($R^2 = 0.997$) as shown in Fig. 3B.

The sensitivity was also excellent: the limit of detection (LOD), calculated as 3 s/m where "s" is the standard deviation of the intercept and "m" is the slope of the regression line in the linear range, was indeed 0.40 ± 0.04 pg mL^{-1} (n = 3) (**Fig. S13**, **Table S5**). Selectivity of the nanoMIPs-PFOA sensor was studied using other PFAS compounds, such as PFBS, PFNA, PFOS, PFPeA. Fig. 4 shows sensor responses to solutions containing 4 pg mL^{-1} of PFOA in the presence of 10-fold concentration (40 pg mL^{-1}) of the different PFAS. These results demonstrate that the presence of these similar compounds had no significant effect on the electrochemical response as the PFOA target was not hindered in binding to the imprinted nanoparticles. This confirmed the strong selectivity of the nanoMIP sensor. Moreover, selectivity does not appear to be related to chain length (PFPeA and PFNA) or to the presence of different functional groups (PFBS and PFOS). It is reasonable to hypothesise that the initial experimental design, which facilitated the production of very small nanoparticles, allowed both good recognition properties and selectivity to be achieved. In fact, as can be seen from **Fig. S1**, the interactions with the target occur via the oxygen of the carboxyl group of PFOA and the monomers ITA and HEM. For this reason, the presence of interferents such as PFOS and PFBS that do not have carboxyl groups appear not to affect the sensor responses. As regards PFPeA and PFNA, which have a chain of 5 and 10 carbon atoms respectively, they produce an increase in the measured standard deviation: the presence of the carboxyl group facilitates binding to the nanoparticle cavities to a certain extent, thereby affecting their swelling.

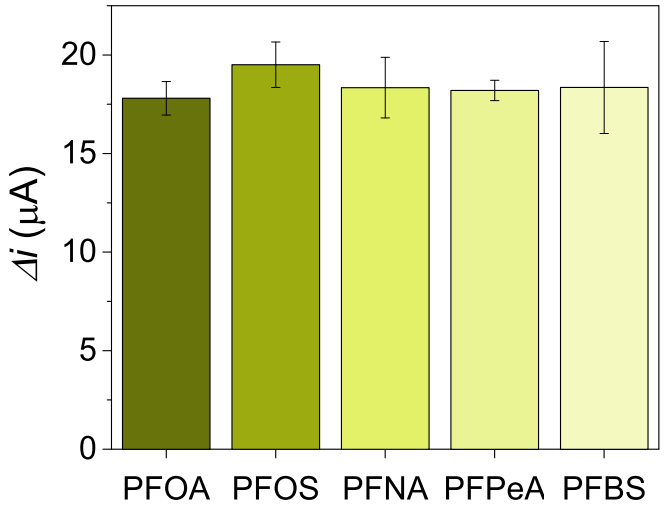

Fig. 4. Selectivity of the sensor to PFOA (4 pg mL^{-1}) in the presence of selected PFAS standards at 10-fold higher concentrations (40 pg mL^{-1}). Error bars represent the standard deviation of three replicates ($n = 3$).

The nanoMIP-PFOA sensor showed good stability and repeatability: five consecutive measurements to 4 pg mL^{-1} PFOA dissolved in PBS (pH = 7.4) taken over 8 h gave a relative standard deviation (RSD) as low as 1.0 %, proving the sensor stability (**Fig. S14A**). Sensor inter-electrode reproducibility was also studied: the RSD of the current response to 50 pg mL^{-1} PFOA of four different nanoMIP-PFOA sensors was 3.4 % (**Fig. S14B**).

In order to assess the accuracy of the nanoMIP-PFOA sensor, recoveries at different levels of PFOA concentration have been measured by spiking the analyte in tap water, diluted 1:10 with PBS. DPV measurements (**Fig. S15**) showed recoveries of 113 %, calculated as found/added per cent, at the lowest and 100 % at the highest spike concentrations (**Table 1**), confirming the accuracy of the proposed sensor to quantify PFOA in water samples.

3.6. Regeneration study

Regeneration of the sensing surface to make the sensor reusable, was achieved using 5 mM PBS pH 7.4 at 65 °C for 20 min. The removal of the template occurred without damaging the APTES layer and the nanoparticles anchored on it. Lower temperatures were ineffective, whereas longer times were detrimental for analyte response after regeneration (results not shown). The height peak for the baseline for non-

Table 1
PFOA recovery of nanoMIPs-PFOA sensor in tap water.

	[PFOA]added, pg mL^{-1}	[PFOA] found, pg mL^{-1}	Recovery (%)
Spiked tap water	1	1.1 ± 0.4	113
	5	5.0 ± 0.5	100

regenerated and regenerated sensors were 45.0 and 40.8 μA, respectively, so the calculated recovery of the baseline current was approximately 90 % (Fig. 5A). However, after the regeneration of the sensor, the same analytical performance could be obtained as the calculated signal recovery was between 94 and 107 % of PFOA current response before regeneration (Fig. 5B). The signal response is therefore stable even after regeneration and comparable with the responses obtained before regeneration, so reusability further lowers overall cost of the presented sensor.

3.7. Application of the nanoMIPs-PFOA sensor on a contaminated sample

On-site sensing measurements were conducted using a commercial portable device equipped with the nanoMIPs-PFOA sensor. To ensure accurate analysis, pH control of the samples was necessary, requiring pre-treatment prior to measurement. Specifically, a contaminated surface water sample collected near an industrial site in the Netherlands (characterized by a PFOA concentration of 50 pg mL^{-1} as determined by LC-MS/MS) was analyzed. The sample was diluted 1:10 with phosphate-buffered saline (PBS) to adjust the pH to the optimal working condition and to bring the PFOA concentration within the linear detection range of the sensor.

Measurements were performed at room temperature, which facilitates simplified field operations. The sensor's response was comparable to that obtained under laboratory conditions with a calibrated potentiostat, although slight differences were noted due to variations in the portable device specifications. A current difference of 26.3 μA was recorded, corresponding to a calculated PFOA concentration of approximately 4.85 pg mL^{-1}. Accounting for the 1:10 dilution, the recovery rate was determined to be 97 %, confirming the sensor's accuracy and reliability for surface water analysis in field conditions.

Compared with other sensor methods (Table 2), the present sensor shows satisfactory performances and has promising potential for application in monitoring the PFOA levels in environmental samples.

3.8. Outlook on method portability for on-site application

For the investigation of PFOA contamination directly in the field, a handheld device is preferred for ease of use and mobility. To simulate an on-site, point-of-need experiment, a preliminary test was conducted which could be directly transferred to real-world on-site applications. The portable on-site equipment setup consisted of the PalmSens Sensit Smart (PalmSens4, Dordrecht, The Netherlands), the world's smallest commercial potentiostat (dimensions: 2.5 × 4.2 cm), and an Android smartphone (Samsung Galaxy A52 5G) equipped with dedicated software (PStouch v2.8) (**Fig. S16A**). These on-site experiments followed the same protocols as those performed previously on the PalmSens 4 potentiostat, utilizing identical functionalized SPEs. A range of PFOA standard solutions was analyzed with both the PalmSens 4 and Sensit Smart on the same day. The data acquired from the Sensit Smart connected to Android phone and the PalmSens 4 was evaluated by constructing dose-response curves using 5 parameter logistics. Both dose-response curves were evaluated by plotting them in the same graph (**Fig. S16B**). These results demonstrated that both potentiostats detected PFOA with comparable sensitivity during measurements on the same day, under identical external conditions (temperature, humidity), indicating that on-site measurements are feasible using miniaturized potentiostats with direct smartphone readout.

Table 2
Analytical performance of the proposed sensor is compared with PFOA-sensors monitoring.

Method	Recognition Element	Linear Range (pg mL^{-1})	LOD (pg mL^{-1})	Reference
Electrochemical	Au/ Cu2O@C@NiCo2O4/ MIP	207–4140	19.5	[39]
Optical	PFOA–MIP	1–750	0.8	[40]
Fluorescence	ssDNA aptamer/PFOA	0–3.1 $x\ 10^7$	70.3	[41]
Thermal	MIP polyacrylamide	4.14–41.4	9.1	[42]
Electrochemical	PFDT/AuNPs/GCE	100–5000	68	[43]
Fluorescence	(PDI) based MOF	2.1–20.7	1.3	[44]
PEC-EC	ZnCdS@$ZnIn_2S_4$	2.1–414.0	0.6	[45]
Electrochemical	nanoMIP/APTES/ SPPtE	1–7.5	0.4	This work

4. Conclusions

In this work, we present a novel approach for detecting perfluorooctanoic acid (PFOA) contaminants by electroactive nanoMIPs, as both sensing and reporting elements, using voltammetric sensors. Through systematic optimization strategies, smaller nanoparticles were synthesized with enhanced sensitivity and selectivity. The size distribution of the nanoMIPs, predicted by experimental design models, was validated using dynamic light scattering (DLS) and transmission electron microscopy (TEM), confirming a homogeneous nanoparticle distribution. The sensor performances were validated. Additionally, a sustainable method for sensor regeneration was proposed. Thanks to its

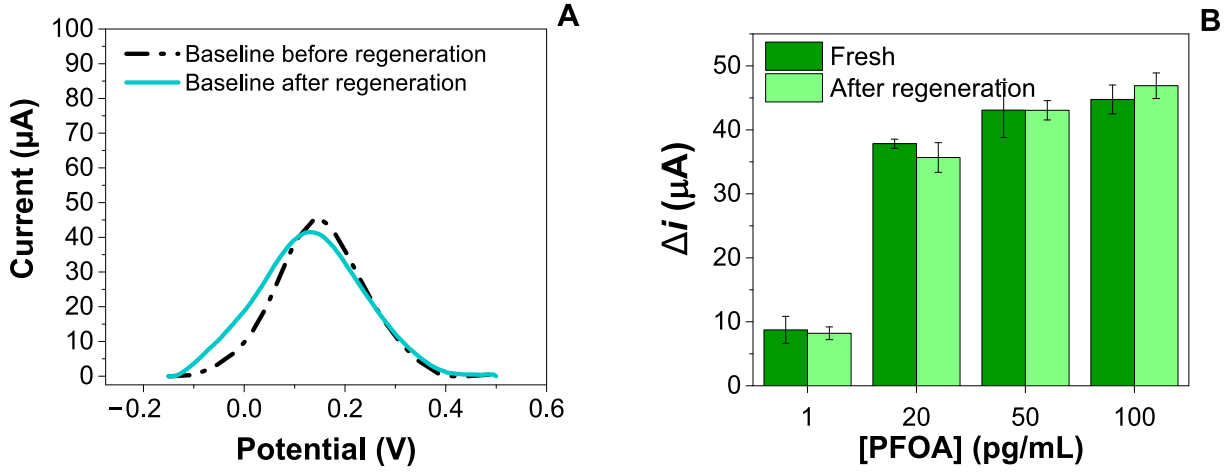

Fig. 5. (A) Baseline of the sensor before (black dash-dot line) and after (green solid line) regeneration of the sensor in 5 mM PBS (pH 7.4) at 65 °C for 20 min; (B) Comparison of sensor responses for PFOA calibration standards before and after regeneration. Error bars represent the standard deviation of three replicates ($n = 3$). (For interpretation of the references to colour in this figure legend, the reader is referred to the web version of this article.)

selectivity for PFOA, the developed sensor demonstrated its potential for PFOA quantification, achieving satisfactory analytical results at the pg mL^{-1} level and in the analysis of a contaminated sample from an industrial site in the Netherlands. This study highlights the potential of nanoMIP-based electrochemical sensors as a reliable and efficient tool for monitoring in environmental samples, and shows that the on-site screening with handheld devices is practicable, avoiding expensive, time-consuming laboratory experiments. Finally, the methods can be scaled up and extended by developing other PFAS nano-MIPS sensors. This work stands out for the integration of multiple innovative elements in a single platform: *(i)* synthesis of electroactive nanoMIPs for the direct PFOA detection; *(ii)* the use of a chemometric approach to optimize and control the synthesis; *(iii)* a miniaturized set-up and smartphone-based analysis; and finally, *(iv)* the possibility of regenerating the sensor.

CRediT authorship contribution statement

Marco Costa: Writing – original draft, Investigation, Data curation. **Sabrina Di Masi:** Writing – original draft, Methodology, Conceptualization. **Christopher Zaleski:** Methodology, Investigation. **Alvaro Garcia Cruz:** Writing – review & editing, Methodology, Investigation. **Erik Beij:** Methodology, Investigation. **Jeroen Peters:** Writing – review & editing, Resources. **Sergey A. Piletsky:** Writing – review & editing, Supervision, Resources. **Cosimino Malitesta:** Writing – review & editing, Supervision, Resources. **Giuseppe Egidio De Benedetto:** Writing – review & editing, Supervision, Data curation.

Funding

Authors would like to thank the financial support of Ph.D. programs “Green Analytical Chemistry: Development of Molecularly Imprinted Polymers for Emerging Pollutants” funded by “Dottorati su tematiche Green del PON R&I 2014–2020 (CUP:F85F21005750001)″.

Declaration of competing interest

The authors declare that they have no known competing financial interests or personal relationships that could have appeared to influence the work reported in this paper.

Acknowledgement

The authors would like to thank Natalie Susan Allcock from the University of Leicester (UK) for providing the TEM images.

Appendix A. Supplementary data

Supplementary data to this article can be found online at https://doi.org/10.1016/j.microc.2025.114645.

Data availability

Data will be made available on request.

References

[1] A.B. Lindstrom, M.J. Strynar, E.L. Libelo, Polyfluorinated compounds: past, present, and future, Environ. Sci. Technol. 45 (2011) 7954–7961.
[2] M.N. Ehsan, M. Riza, M.N. Pervez, C.-W. Li, A.A. Zorpas, V.J. Naddeo, PFAS contamination in soil and sediment: contribution of sources and environmental impacts on soil biota, Case Studies in Chemical Environmental Engineering 9 (2024) 100643.
[3] J.D. Boettger, N.M. DeLuca, M.A. Zurek-Ost, K.E. Miller, C. Fuller, K.D. Bradham, P. Ashley, W. Friedman, E.A. Pinzer, D.C. Cox, Emerging per-and Polyfluoroalkyl Substances in Tap Water from the American Healthy Homes Survey II, Environmental Science Technology, 2025.
[4] J.-C. Liou, B. Szostek, C. DeRito, E. Madsen, Investigating the biodegradability of perfluorooctanoic acid, Chemosphere 80 (2010) 176–183.
[5] S. Vaalgamaa, A.V. Vähätalo, N. Perkola, S. Huhtala, Photochemical reactivity of perfluorooctanoic acid (PFOA) in conditions representing surface water, Sci. Total Environ. 409 (2011) 3043–3048.
[6] X.C. Hu, A.K. Tokranov, J. Liddie, X. Zhang, P. Grandjean, J.E. Hart, F. Laden, Q. Sun, L.W. Yeung, E.M. Sunderland, Tap water contributions to plasma concentrations of poly-and perfluoroalkyl substances (PFAS) in a nationwide prospective cohort of US women, Environ. Health Perspect. 127 (2019) 067006.
[7] S.C.E. Leung, P. Shukla, D. Chen, E. Eftekhari, H. An, F. Zare, N. Ghasemi, D. Zhang, N.-T. Nguyen, Q. Li, Emerging technologies for PFOS/PFOA degradation and removal: a review, Sci. Total Environ. 827 (2022) 153669.
[8] M. Al Amin, Z. Sobhani, Y. Liu, R. Dharmaraja, S. Chadalavada, R. Naidu, J. M. Chalker, C. Fang, Recent advances in the analysis of per-and polyfluoroalkyl substances (PFAS)—a review, Environ. Technol. Innov. 19 (2020) 100879.
[9] Q. Pan, H. Zhang, Q. Liu, D. Huang, D.-P. Yang, T. Jiang, S. Sun, X. Chen, A self-powered cathodic molecular imprinting ultrasensitive photoelectrochemical tetracycline sensor via ZnO/C photoanode signal amplification, Chin. Chem. Lett. 36 (2025) 110169.
[10] Y.-F. Yang, Y.-J. Feng, X.-P. Hu, H.-W. Gu, X.-F. Yan, X.-L. Yin, Smartphone-based visual sensing platform based on molecular imprinted polymers and aptamers synergistic recognition for simultaneous detection of aflatoxin B1 and ochratoxin a, Microchem. J. 212 (2025) 113361.
[11] C. Dincer, R. Bruch, E. Costa-Rama, M.T. Fernández-Abedul, A. Merkoçi, A. Manz, G.A. Urban, F. Güder, Disposable sensors in diagnostics, food, and environmental monitoring, Adv. Mater. 31 (2019) 1806739.
[12] V. Naresh, N. Lee, A review on biosensors and recent development of nanostructured materials-enabled biosensors, Sensors 21 (2021) 1109.
[13] M. Arabi, A. Ostovan, J. Li, X. Wang, Z. Zhang, J. Choo, L. Chen, Molecular imprinting: green perspectives and strategies, Adv. Mater. 33 (2021) 2100543.
[14] M. Arabi, A. Ostovan, Y. Wang, R. Mei, L. Fu, J. Li, X. Wang, L. Chen, Chiral molecular imprinting-based SERS detection strategy for absolute enantiomeric discrimination, Nat. Commun. 13 (2022) 5757.
[15] A. Ostovan, M. Arabi, Y. Wang, J. Li, B. Li, X. Wang, L. Chen, Greenificated molecularly imprinted materials for advanced applications, Adv. Mater. 34 (2022).
[16] F. Truta, A.G. Cruz, M. Tertis, C. Zaleski, G. Adamu, N.S. Allcock, M. Suciu, M.-G. Ștefan, B. Kiss, E. Piletska, NanoMIPs-based electrochemical sensors for selective detection of amphetamine, Microchem. J. 191 (2023) 108821.
[17] F. Canfarotta, J. Czulak, A. Guerreiro, A.G. Cruz, S. Piletsky, G.E. Bergdahl, M. Hedström, B. Mattiasson, A novel capacitive sensor based on molecularly imprinted nanoparticles as recognition elements, Biosens. Bioelectron. 120 (2018) 108–114.
[18] F. Canfarotta, A. Poma, A. Guerreiro, S. Piletsky, Solid-phase synthesis of molecularly imprinted nanoparticles, Nat. Protoc. 11 (2016) 443–455.
[19] M. Sandhya, D. Ramasamy, K. Sudhakar, K. Kadirgama, W. Harun, Ultrasonication an intensifying tool for preparation of stable nanofluids and study the time influence on distinct properties of graphene nanofluids–a systematic overview, Ultrason. Sonochem. 73 (2021) 105479.
[20] R. Say, M. Erdem, A. Ersöz, H. Türk, A. Denizli, Biomimetic catalysis of an organophosphate by molecularly surface imprinted polymers, Appl. Catal. A Gen. 286 (2005) 221–225.
[21] D. Lakshmi, A. Bossi, M.J. Whitcombe, I. Chianella, S.A. Fowler, S. Subrahmanyam, E.V. Piletska, S.A. Piletsky, Electrochemical sensor for catechol and dopamine based on a catalytic molecularly imprinted polymer-conducting polymer hybrid recognition element, Anal. Chem. 81 (2009) 3576–3584.
[22] E. Toorisaka, K. Uezu, M. Goto, S. Furusaki, A molecularly imprinted polymer that shows enzymatic activity, Biochem. Eng. J. 14 (2003) 85–91.
[23] T. Cowen, K. Karim, S. Piletsky, Computational approaches in the design of synthetic receptors–a review, Anal. Chim. Acta 936 (2016) 62–74.
[24] S. Di Masi, G.E. De Benedetto, C. Malitesta, Optimisation of electrochemical sensors based on molecularly imprinted polymers: from OFAT to machine learning, analytical bioanalytical, Chemistry 416 (2024) 2261–2275.
[25] D. Refaat, M.G. Aggour, A.A. Farghali, R. Mahajan, J.G. Wiklander, I.A. Nicholls, S. A. Piletsky, Strategies for molecular imprinting and the evolution of MIP nanoparticles as plastic antibodies—synthesis and applications, Int. J. Mol. Sci. 20 (2019) 6304.
[26] M. Abyadeh, A.A.K. Zarchi, M.A. Faramarzi, A. Amani, Evaluation of factors affecting size and size distribution of chitosan-electrosprayed nanoparticles, Avicenna journal of medical biotechnology 9 (2017) 126.
[27] N. Bock, T.R. Dargaville, M.A. Woodruff, Electrospraying of polymers with therapeutic molecules: state of the art, Prog. Polym. Sci. 37 (2012) 1510–1551.
[28] J.-F. Hu, S.-F. Li, G.R. Nair, W.-T. Wu, Predicting chitosan particle size produced by electrohydrodynamic atomization, Chem. Eng. Sci. 82 (2012) 159–165.
[29] D.V.H. Thien, S.W. Hsiao, M.H. Ho, Synthesis of electrosprayed chitosan nanoparticles for drug sustained release, Nano Life 2 (2012) 1250003.
[30] S. Zhang, K. Kawakami, One-step preparation of chitosan solid nanoparticles by electrospray deposition, Int. J. Pharm. 397 (2010) 211–217.
[31] M. Wagner, A. Krieger, F. Gröhn, Gold nanoparticles in disulfide based polymer matrices: size, Structure and Responsivity, Macromolecular Chemistry Physics 225 (2024) 2300342.
[32] Y. Xiong, Y. Wang, H. Wang, R. Wang, A facile one-step synthesis to ionic liquid-based cross-linked polymeric nanoparticles and their application for CO 2 fixation, Polym. Chem. 2 (2011) 2306–2315.
[33] S. Clarke, Development of Hierarchical Magnetic Nanocomposite Materials for Biomedical Applications, Dublin City University, 2013.
[34] S.K. Vashist, Comparison of 1-ethyl-3-(3-dimethylaminopropyl) carbodiimide based strategies to crosslink antibodies on amine-functionalized platforms for immunodiagnostic applications, Diagnostics 2 (2012) 23–33.

[35] S. Udomsom, U. Mankong, P. Paengnakorn, N. Theera-Umpon, Novel rapid protein coating technique for silicon photonic biosensor to improve surface morphology and increase bioreceptor density, Coatings 11 (2021) 595.
[36] Q. Shao, C.K. Hall, Allosteric effects of gold nanoparticles on human serum albumin, Nanoscale 9 (2017) 380–390.
[37] I. Haq, A.G. Cruz, S. Di Masi, T. Cowen, N.S. Allcock, C. Malitesta, A. Mujahid, T. Hussain, E. Piletska, S.A. Piletsky, Smart nano-actuators for electrochemical sensing of metformin in human plasma, Sensors Actuators B Chem. 376 (2023) 132928.
[38] Q. Yu, S. Deng, G. Yu, Selective removal of perfluorooctane sulfonate from aqueous solution using chitosan-based molecularly imprinted polymer adsorbents, Water Res. 42 (2008) 3089–3097.
[39] Y. Wei, H. Liu, S. Wang, K. Yu, L. Wang, A portable molecularly imprinted polymer-modified microchip sensor for the rapid detection of perfluorooctanoic acid, Analyst 148 (2023) 3851–3859.
[40] R. Pitruzzella, F. Arcadio, C. Perri, D. Del Prete, G. Porto, L. Zeni, N. Cennamo, Ultra-low detection of perfluorooctanoic acid using a novel plasmonic sensing approach combined with molecularly imprinted polymers, Chemosensors 11 (2023) 211.
[41] J. Park, K.-A. Yang, Y. Choi, J.K. Choe, Novel ssDNA aptamer-based fluorescence sensor for perfluorooctanoic acid detection in water, Environ. Int. 158 (2022) 107000.
[42] F.A. Tabar, J.W. Lowdon, M. Caldara, T.J. Cleij, P. Wagner, H. Diliën, K. Eersels, B. van Grinsven, Thermal determination of perfluoroalkyl substances in environmental samples employing a molecularly imprinted polyacrylamide as a receptor layer, Environ. Technol. Innov. 29 (2023) 103021.
[43] J.J.C. Solís, S. Yin, M. Galicia, M.S. Ersan, P. Westerhoff, D. Villagrán, "Forever chemicals" detection: a selective nano-enabled electrochemical sensing approach for perfluorooctanoic acid (PFOA), Chem. Eng. J. 491 (2024) 151821.
[44] R. Dalapati, M. Hunter, M. Sk, X. Yang, L. Zang, Fluorescence turn-on detection of perfluorooctanoic acid (pfoa) by perylene diimide-based metal–organic framework, ACS Appl. Mater. Interfaces 16 (2024) 32344–32356.
[45] H. Zheng, L. Bai, C. Du, X. Zhang, J. Chen, PEC-EC Dual-Mode Biosensing Platform for PFOA Assay Based on Competitive Binding between HSA and PFOA or Hemin, Sensors Actuators B Chem. (2025) 137326.